Supplementary Information (SI) for Journal of Materials Chemistry A.


# Supplementary Information

## Asymmetrical Sc coordination-induced bridging structure and surface relaxation for boosting $H_2O_2$ photoactivation in Fenton-like catalysis

Cong Liu[a,b], Mingchuan Yu[a*], Yuhao Ma[a], Yuanzheng Zhang[a,c], Yufei Zhou[a], Junfeng Niu[a]

[a] *College of Environmental Science and Engineering, North China Electric Power University, Beijing 102206, China*

[b] *College of Water Conservancy and Hydropower Engineering, North China Electric Power University, Beijing 102206, China*

[c] *State Key Laboratory of Water Environment Simulation, School of Environment, Beijing Normal University, Beijing, China*

* Corresponding author.

E-mail: yumc@ncepu.edu.cn

Tel./fax: +86-10- 61773789

## Synthesis of g-$C_3N_4$

1 g of melamine, 1 g of cyanuric acid and 0.1 g of uramil were added to a solution of ultrapure water and ethanol (volume ratio = 80:20), and stirred for 2 h. The resulting mixture was the dried and the solids were placed into a porcelain boat. A calcination process was carried out at 550°C for 2 h under nitrogen gas at a heating rate of 5°C/min.

## Synthesis of $MoSe_2$

Firstly, two separate solutions, solution A and solution B, were prepared. Solution A: sodium molybdate ($Na_2MoO_4 \cdot 2H_2O$, 2.42 g) was added to ultrapure water (50 mL); solution B: selenium (1.62 g) was added to ultrapure water (50 mL). Then, solution A was slowly added to solution B during stirring to form a mixture. The mixture was transferred into a PTFE reactor and subjected to a hydrothermal reaction at 200°C for 20 h. After cooling to room temperature, the powder was washed with ultrapure water and dried at 40°C in a vacuum oven.

**Tab. S1** Composition of CSM samples

| | CN (g) | Sc precursor (g) | $MoSe_2$ (g) |
|---|---|---|---|
| CSM_1 | 0.2 | 0.01 | 0.01 |
| CSM_2 | 0.2 | 0.01 | 0.02 |
| CSM_3 | 0.2 | 0.01 | 0.03 |
| CSM_4 | 0.2 | 0.005 | 0.02 |
| CSM_5 | 0.2 | 0.02 | 0.02 |

## Characterization

Other characterizations were carried out by transmission electron microscopy (TEM, Tecnai G F20, FEI, USA), X-ray photoelectron spectroscopy (XPS, ESCALAB 250XI, Thermo, USA) and X-ray diffraction spectroscopy (XRD, D8 Advance, Bruker, GER). Transient photocurrent responses and electrochemical impedance spectroscopy (EIS) and photocurrent response tests were conducted using an electrochemical workstation (CHI660E, CHI). A typical three-electrode system was utilized, where a platinum sheet (1 cm × 1 cm) and a saturated calomel electrode (SCE) were used as the counter and reference electrodes, respectively. The working electrodes were prepared by coating the samples inks on nickel foam substrates (1 cm × 1 cm). The ink mixture comprised of solid samples (0.25 g), Nafion solution (0.5 wt%, 10 μL) and ultrapure water (1.0 mL). During testing, a 300 W Xenon lamp (PLS-SXE300, Beijing Perfectlight) with an ultraviolet cut-off filter ($\lambda > 420$ nm) was used as light source. The corresponding parameters in EIS test included a frequency range of 100 kHz to 10 mHz with an amplitude of 5 mV. Electron spin-resonance spectroscopy (ESR, JES FA200, JEOL, JPN) was performed to test the active species.

## Analysis procedures

The concentration of tetrabromobisphenol A (TBBPA) was measured using ultra-high performance liquid chromatography (UPLC, ACQUITY H-class, Waters) with Xbridge BEH C18 column (2.1 mm × 50 mm, 1.7 μm). The wavelength of the PDA detector was set at 278 nm, and the sample injection volume was 1.0 μL. The mobile phase was a mixture of HPLC-grade methanol and formic acid in ultrapure water (0.1%), which was delivered at 0.3 mL/min through the column. A gradient expressed as the ratio of methanol was as follows: 0-1.0 min, 20%; 1.0-1.5 min, a linear increase from 20% to 50%; 1.5-3.0 min, hold at 50%; 3.0-3.5 min, a linear decrease to 20%, and hold at 20% to 5.0 min. The concentration of Br ions was measured by an ion chromatography (IC, ICS-5000+). The intermediates were analyzed using an ultra-high performance liquid chromatography coupled with Orbitrap mass spectrometer (Dionex Ultimate 3000-Q Exactive Foucus, Thermo Fisher) with the electrospray ionization (ESI) source under a negative mode. A full scan mode (m/z 50 to 500) was used, and capillary voltage, cone voltages and desolvation temperature were 3.0 kV, 30 V, and 350°C, respectively. The products ion scan ($MS^2$) was carried out and compound discoverer software was utilized for analysis.

## Theoretical procedure

Density functional theory (DFT) calculaitons, including structural optimization, density of states (DOS), difference charge density and Gibbs free energy, were conducted using Vienna ab initio simulation package (VASP) and projector-augmented wave (PAW) methods.[S1] The correlation interactions were based on the generalized gradient approximation (GGA). The cut-off energy for the calculations was set to 450 eV,[S2,S3] and the force tolerance was set to 0.02 eV/Å. To avoid interaction between the two surfaces, a large vacuum gap of 15 Å was selected in the periodically repeated slabs. The DOS and the difference charge density analyses were performed with a convergence condition of $1.0 \times 10^{-6}$ eV/atom for total energy. The computational hydrogen electrode (CHE) model was used to obtain free energy change.

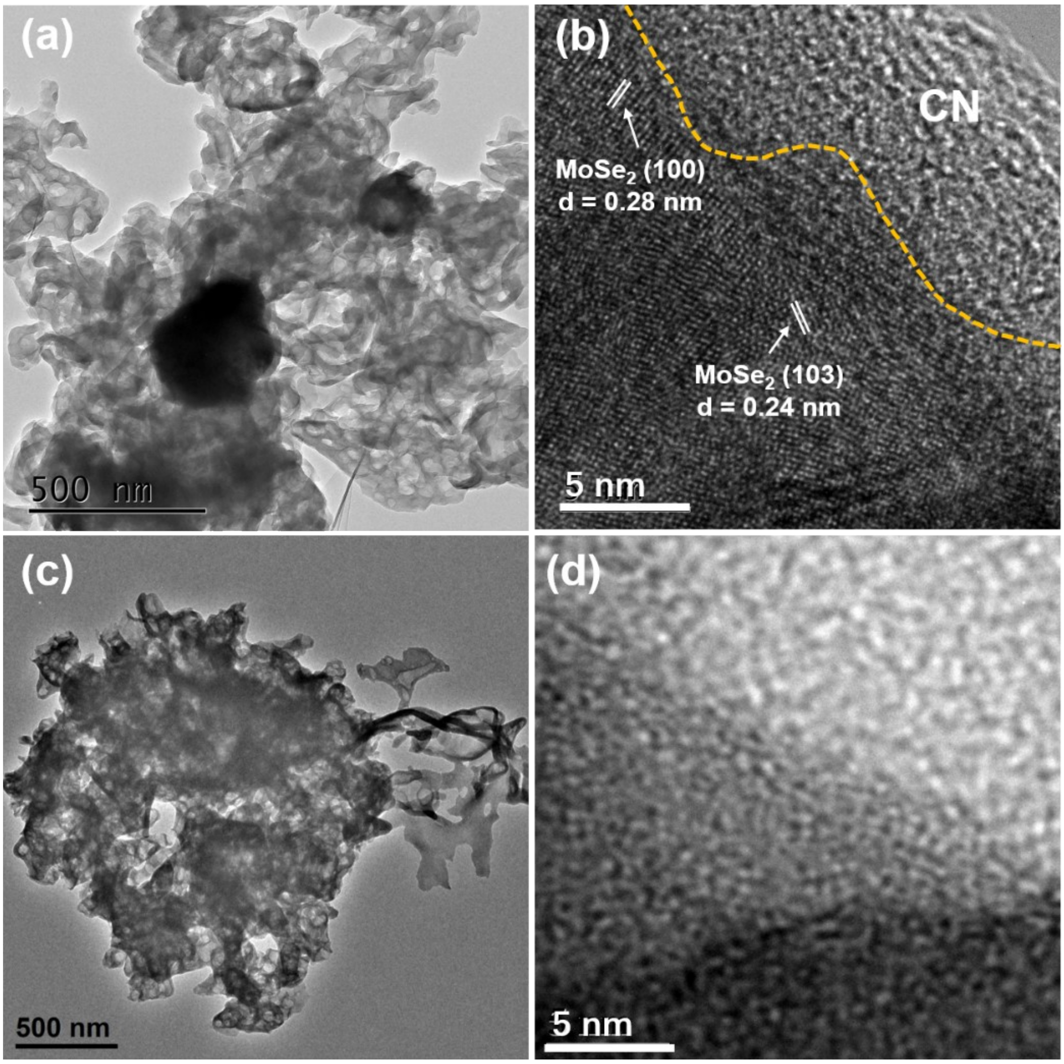


**Fig. S1** HRTEM images of (a-b) CSM_2 and (c-d) CN.

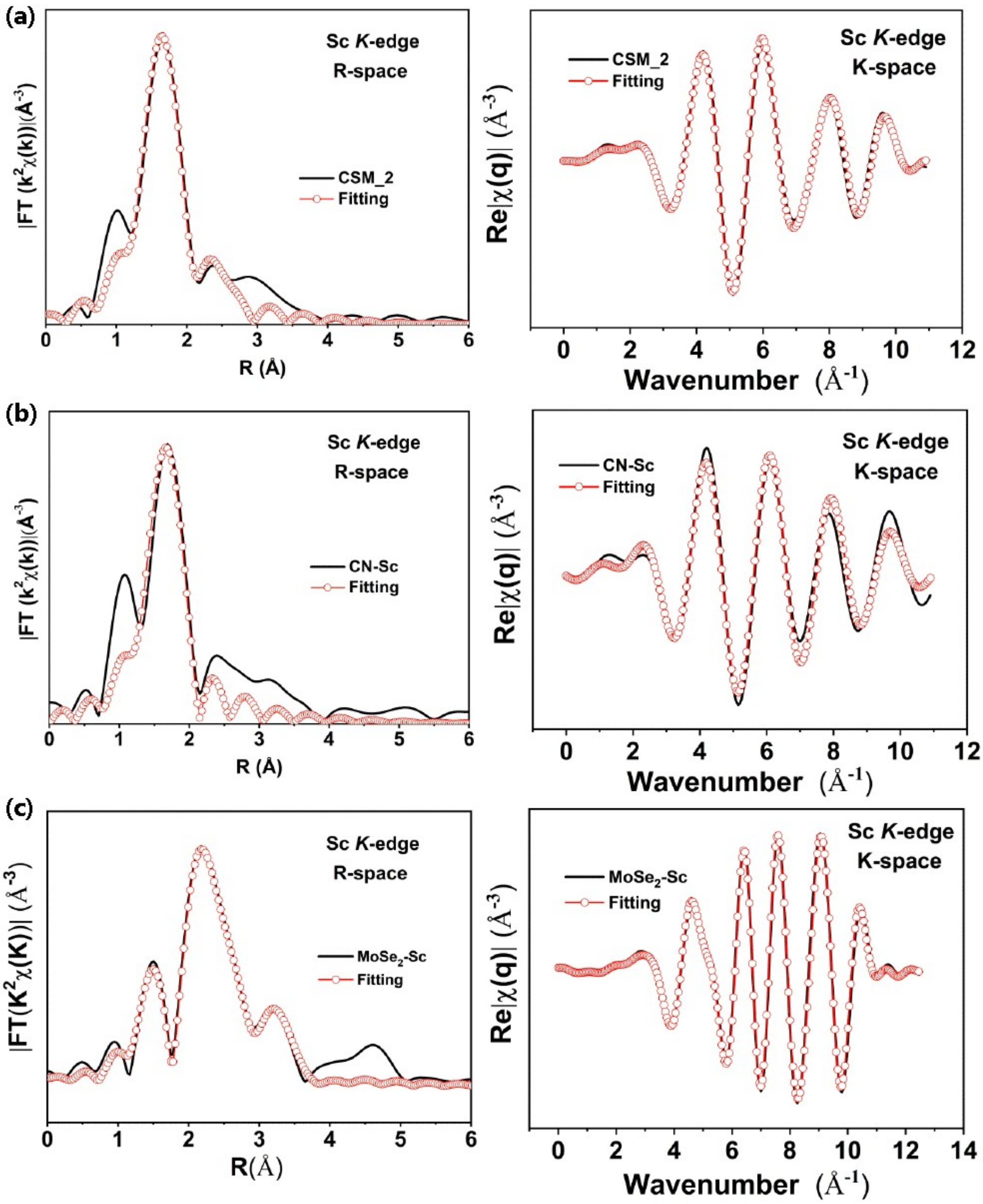


**Fig. S2** EXAFS fitting profiles of the (a) CSM_2, (b) CN-Sc and (c) $MoSe_2$-Sc at Sc K-edge.

**Tab. S2** Structural parameters of the samples obtained from EXAFS fitting.

| Sample | Bond type | N | R (Å) | $\Delta E_0$ (eV) | $\sigma^2 \times 10^3$ (Å$^2$) | R-factor |
|---|---|---|---|---|---|---|
| CSM_2 | Sc-N | 4.0 | 2.12±0.01 | -4.9±3.6 | 6.6±3.2 | 0.008 |
| | Sc-Se | 1.3±0.5 | 2.73±0.01 | 13.6±11.1 | 17.3 | |
| CN-Sc | Sc-N | 5.5±1.7 | 2.13±0.03 | -1.0±3.8 | 6.2±5.1 | 0.036 |

N, coordination number;

R, distance between absorber and backscatter atoms;

$\Delta E_0$, inner potential correction to account for the difference in the inner potential between the sample and the reference compound.

$\sigma^2$, Debye–Waller factor.

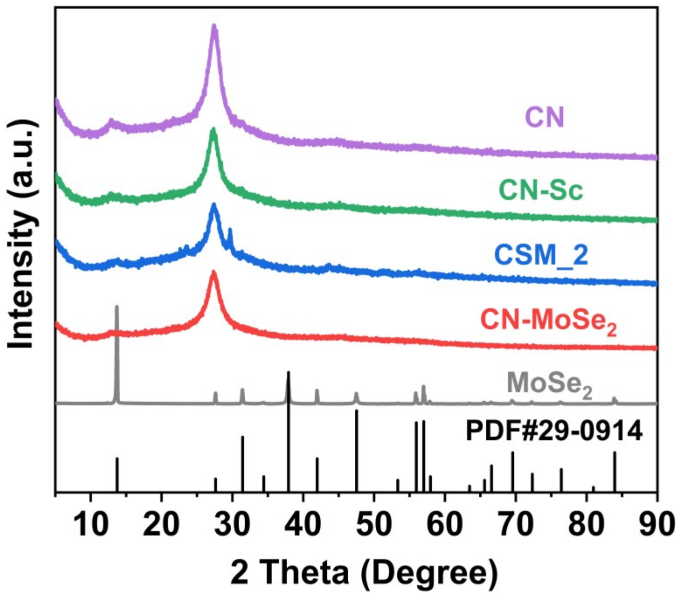


**Fig. S3** XRD patters of the samples.

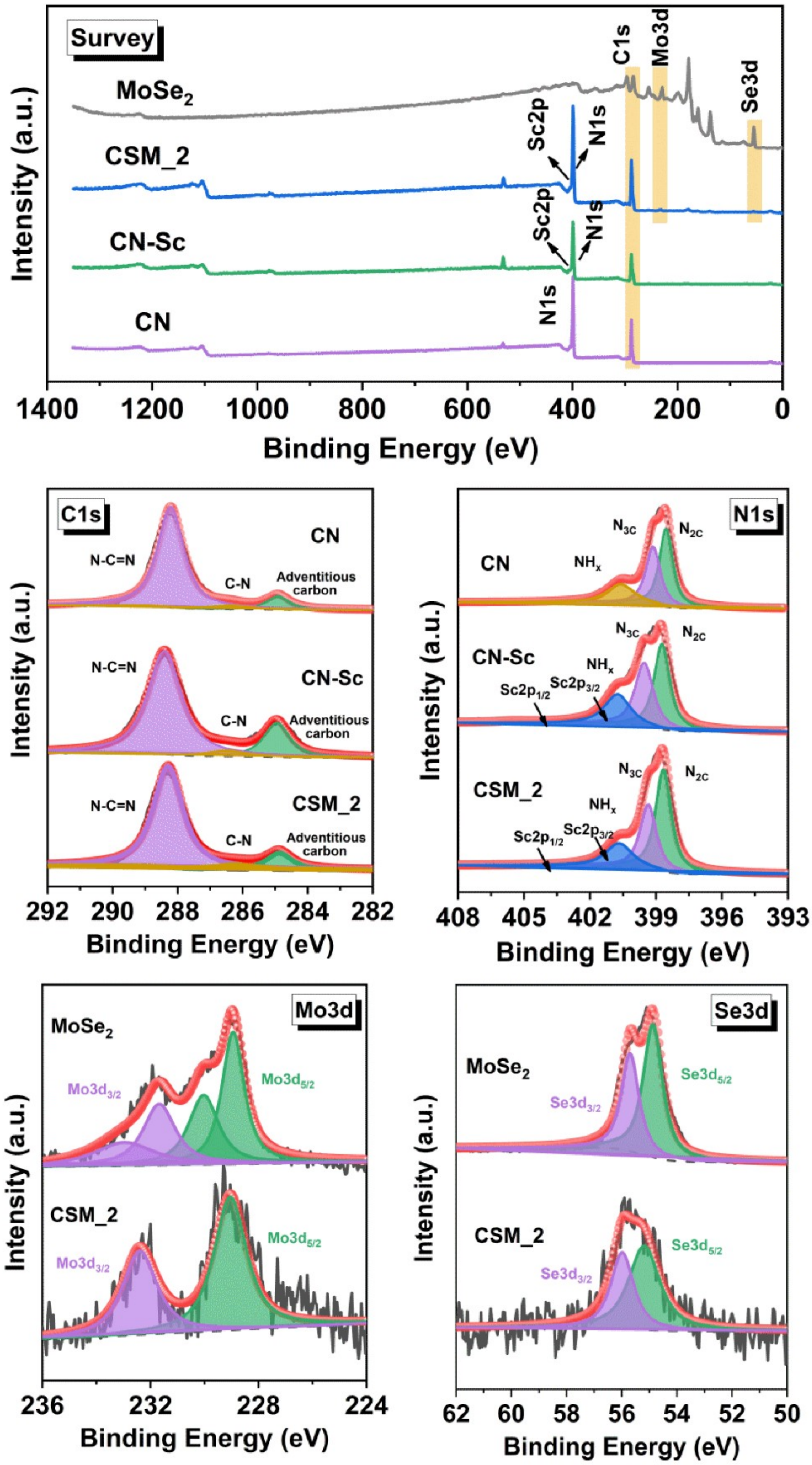


**Fig. S4** Survey, C1s, N1s, Mo3d and Se3d XPS spectra of the samples.

In C1s XPS spectra, the CN-based samples exhibit traditional peaks associated with adventitious carbon (284.8 eV), C–N (286.2 eV) and N–C=N (288.2 eV). In N1s XPS spectra, both CN-Sc and CSM_2 samples show peaks corresponding to Sc2p, with the exception of peaks attributed to bi-coordinated nitrogen ($N_{2C}$, 398.6 eV), tri-coordinated nitrogen ($N_{3C}$, 399.5 eV) and $NH_x$ groups (400.7 eV).[S4-S6] The peaks of $Sc2p_{3/2}$ (400.4 eV) and $Sc2p_{1/2}$ (404.8 eV) are indiscernible due to the low Sc amount and overlapped with nitrogen.[S7] For Mo3d and Se3d XPS spectra, both $MoSe_2$ and CSM_2 exhibit similar peaks corresponding to $Mo3d_{5/2}$, $Mo3d_{3/2}$ and $Se3d_{5/2}$, $Se3d_{3/2}$, respectively.

**Tab. S3** Fitting parameters from TRPL spectra.

| ns [%] | $\tau_1$ [$A_1$] | $\tau_2$ [$A_2$] | $\tau_3$ [$A_3$] | $\tau_{avg}$ |
|---|---|---|---|---|
| CN | 3.44 [30.84] | 1.15 [67.51] | 16.27 [1.66] | 4.24 |
| CN-Sc | 0.60 [46.82] | 10.00 [3.63] | 2.25 [49.55] | 3.59 |
| CN-$MoSe_2$ | 2.79 [34.02] | 0.91 [64.29] | 13.70 [1.69] | 3.60 |
| CSM_2 | 2.66 [37.84] | 12.5 [1.99] | 0.82 [60.17] | 3.54 |

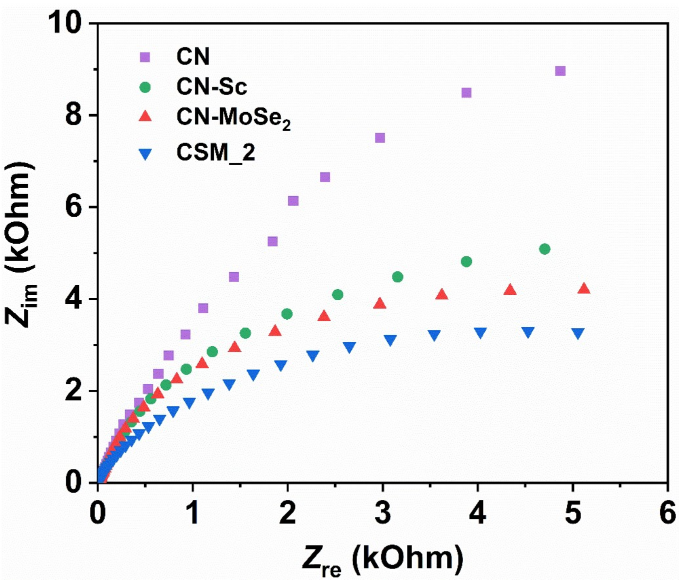


**Fig. S5** EIS spectra of the samples.

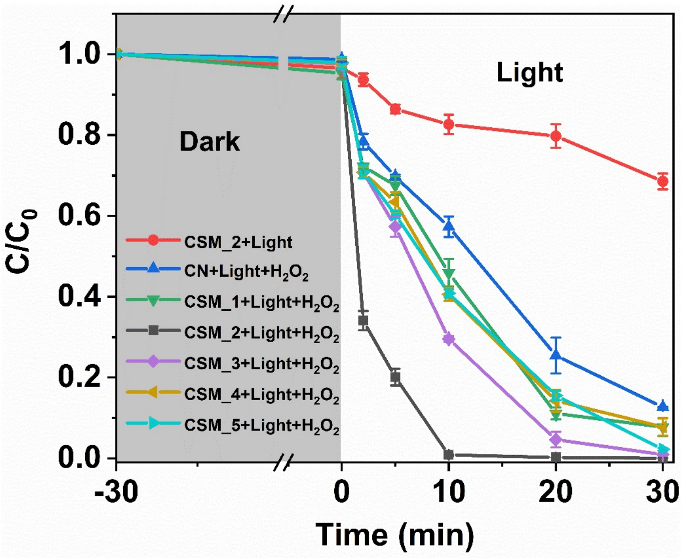


**Fig. S6** Plots of $C/C_0$ versus time of the CSM_2+Light, CN+Light+$H_2O_2$, CSM_1+Light+$H_2O_2$, CSM_2+Light+$H_2O_2$, CSM_3+Light+$H_2O_2$, CSM_4+Light+$H_2O_2$ and CSM_5+Light+$H_2O_2$.

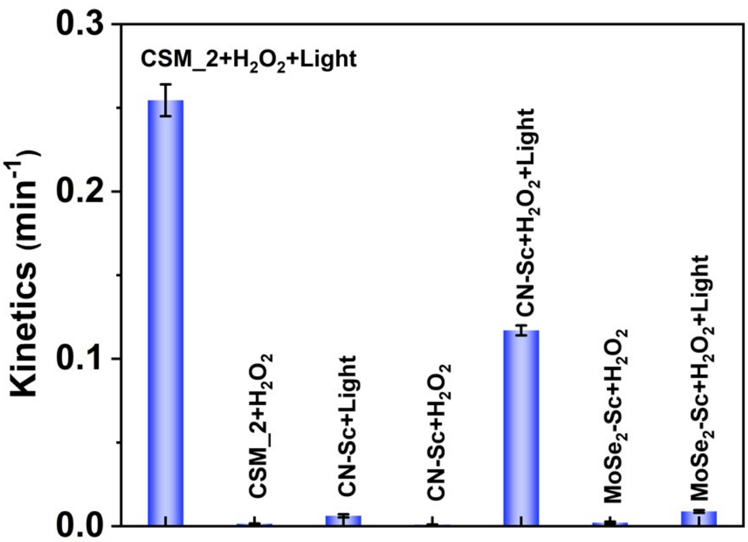


**Fig. S7** Apparent rate constant of the CSM_2+$H_2O_2$, CN-Sc+Light, CN-Sc+$H_2O_2$, CN-Sc+Light+$H_2O_2$, $MoSe_2$-Sc+$H_2O_2$, $MoSe_2$-Sc+$H_2O_2$+Light.

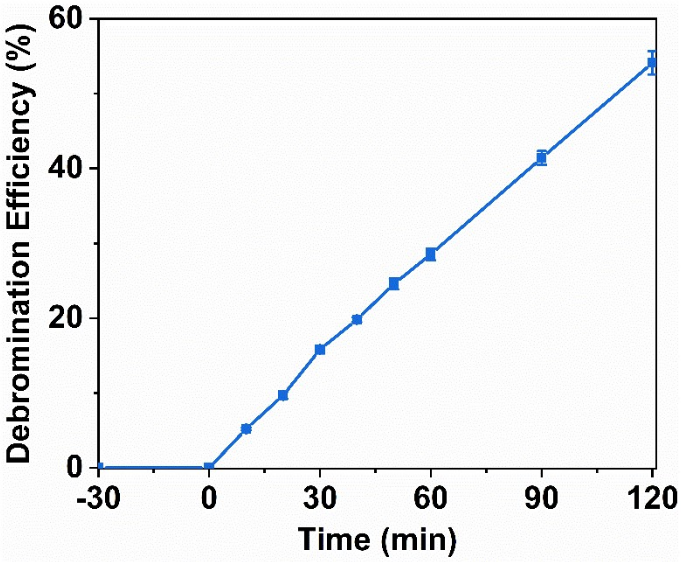


**Fig. S8** Debromination efficiency of the CSM_2-induced photo-Fenton system.

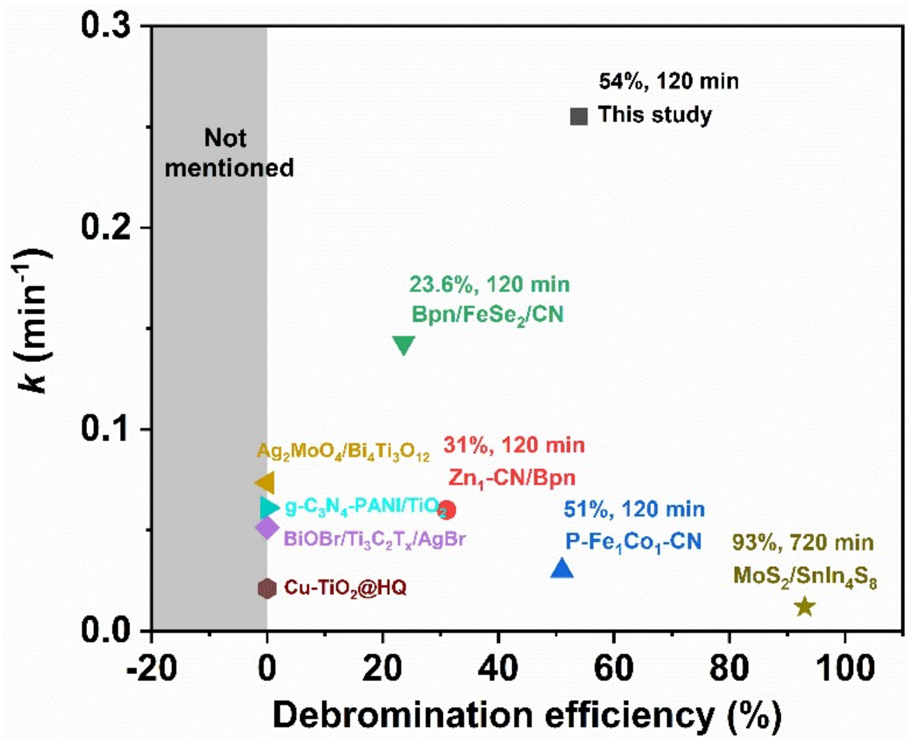


**Fig. S9** Photocatalytic performance of TBBPA degradation over Zn single-atom anchored g-$C_3N_4$/ black phosphorus nanosheets ($Zn_1$-CN/Bpn)[S8], P-induced Fe and Co single-atoms anchored g-$C_3N_4$ (P-$Fe_1Co_1$/CN)[S9], black phosphorus nanosheets/$FeSe_2$/g-$C_3N_4$ (Bpn/$FeSe_2$/CN)[S10], BiOBr/$Ti_3C_2T_x$/AgBr[S11], $Ag_2MoO_4$/$Bi_4Ti_3O_{12}$[S12], Cu-$TiO_2$@8-

Hydroxyquinoline (Cu-$TiO_2$@HQ)[S13], g-$C_3N_4$-PANI/$TiO_2$[S14], $MoS_2$/$SnIn_4S_8$[S15].

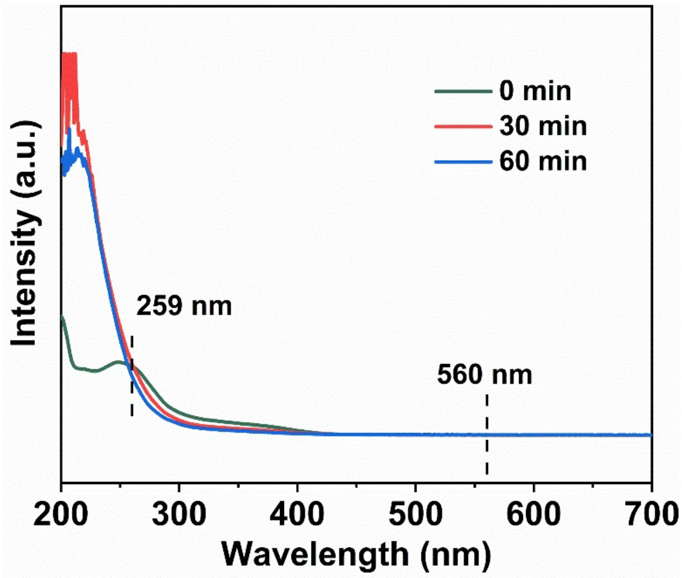


**Fig. S10** Time-dependent UV-vis absorption spectra of NBT solution in CSM_2+Light+$H_2O_2$ system, [NBT] = 0.1 mM.

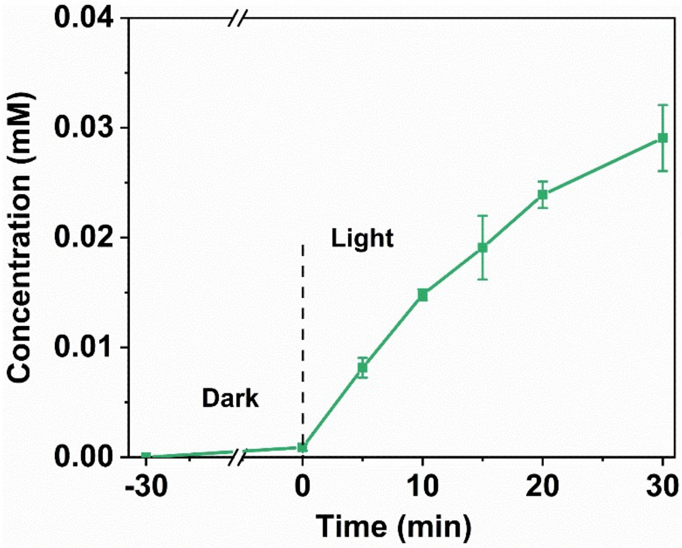


**Fig. S11** •OH production in the CSM_2-induced photo-Fenton-like system by a salicylic acid method.

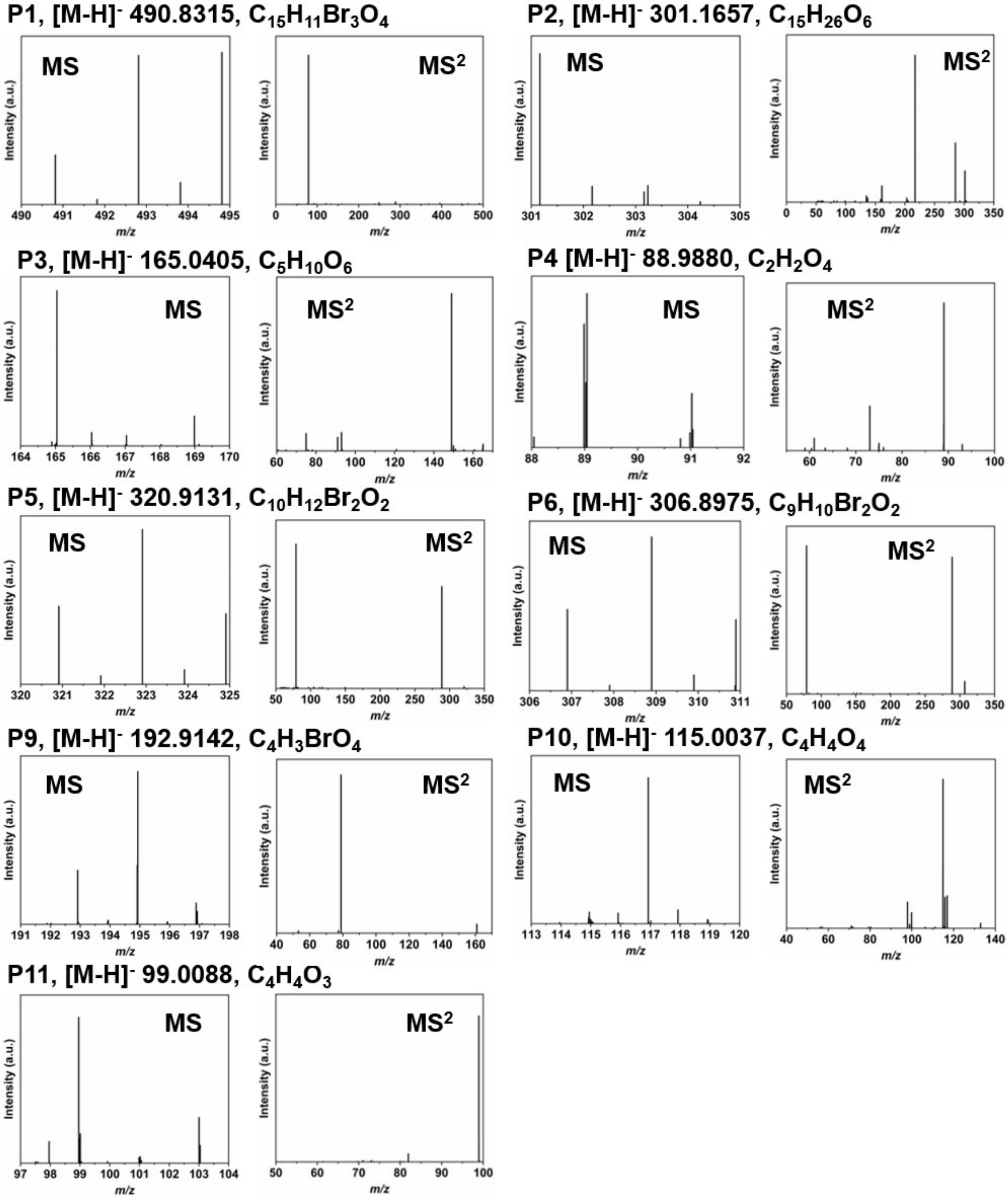


**Fig. S12** MS and $MS^2$ spectra of the intermediate products in CSM_2-induced photo-Fenton-like system.

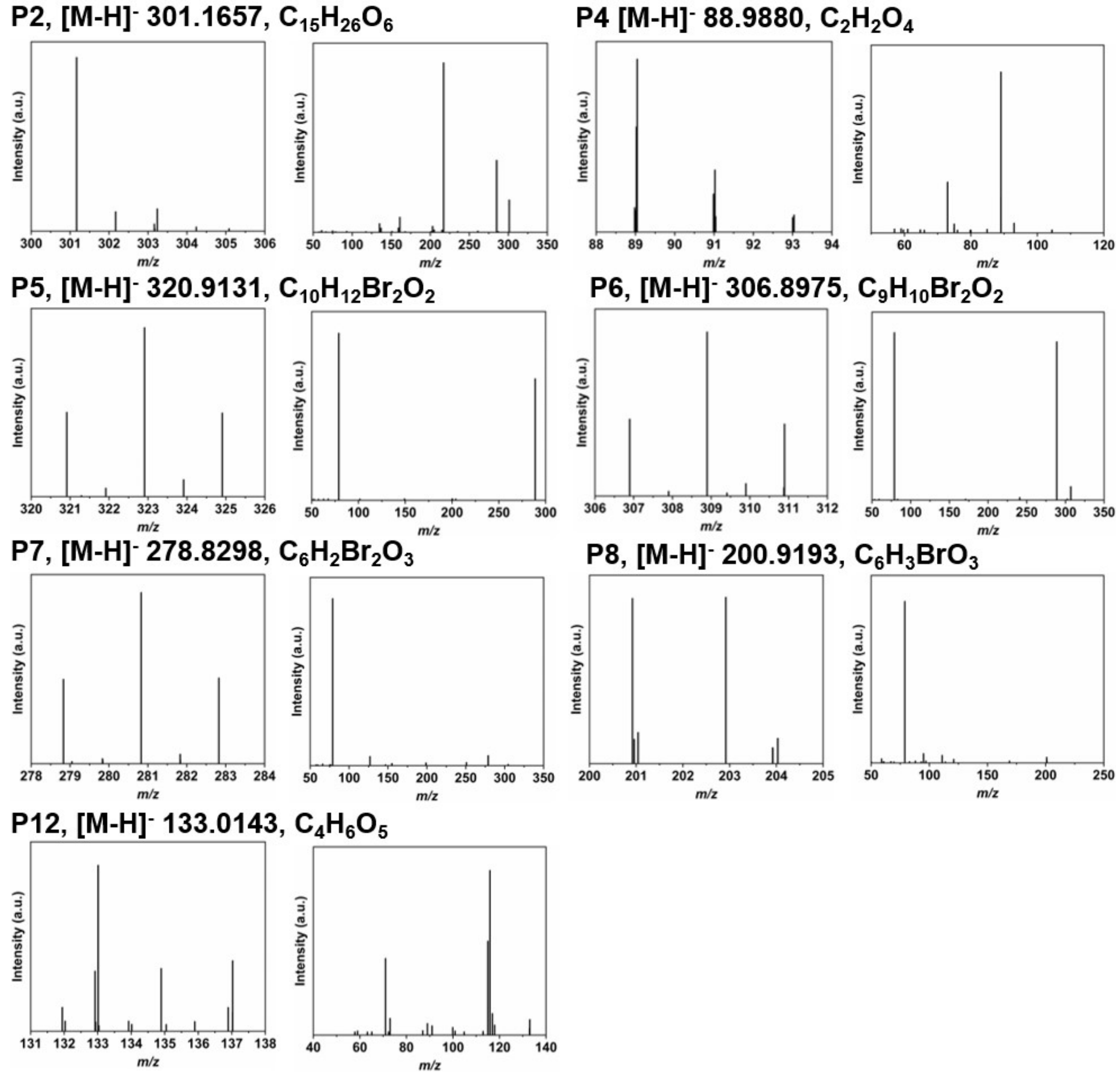


**Fig. S13** MS and MS$^2$ spectra of the intermediate products in CSM_2-induced pure photocatalytic system.

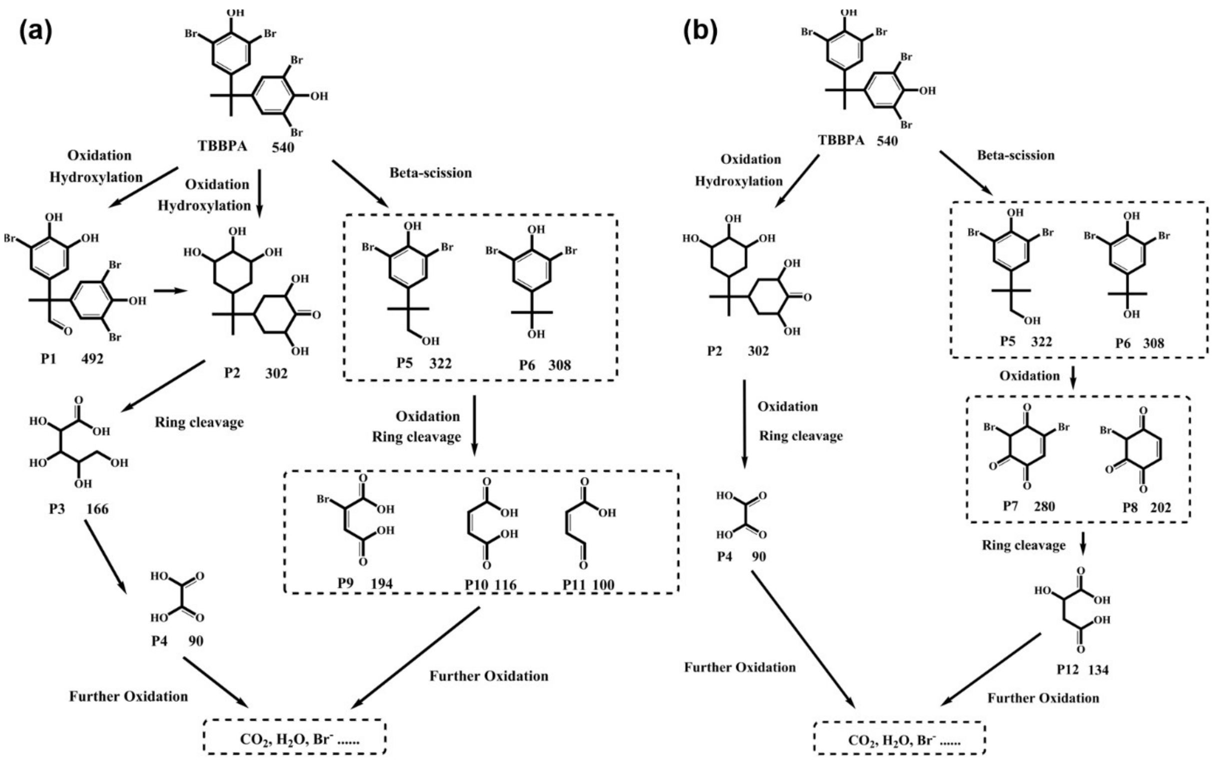


**Fig. S14** Proposed degradation routes in the CSM_2-induced (a) photo-Fenton-like system and (b) pure photocatalytic system.

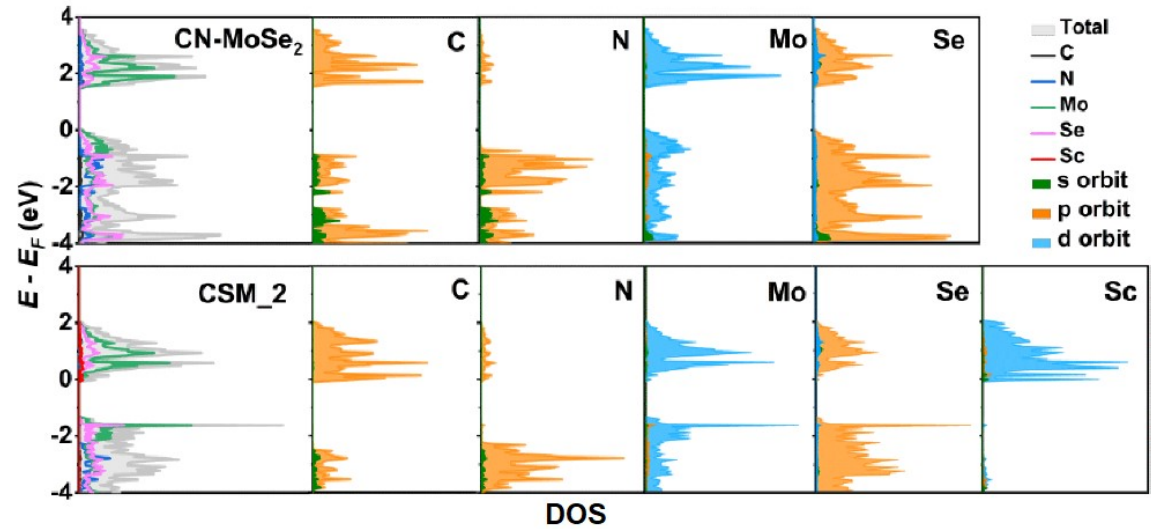


**Fig. S15** DOS profiles of the CN-MoSe2 and CSM_2.

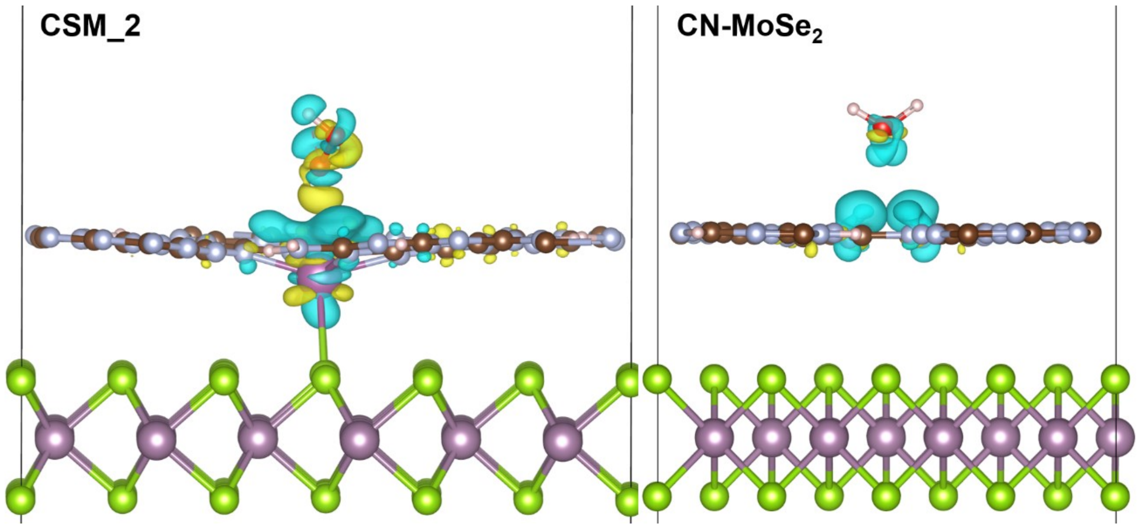


**Fig. S16** Difference charge density profiles of the adsorbed $H_2O_2$ on the (a) CSM_2 and (b) CN-$MoSe_2$, yellow and cyan represent accumulation and depletion charge areas, respectively.

**Tab. S4** Bader charge transfer (Δq) in CSM_2.

| Atom | Δq |
|---|---|
| 1O | 0.023353 |
| 2O | 0.006041 |
| 3H | -0.004545 |
| 4H | -0.00758 |
| 5N | -0.105924 |
| 6N | -0.080391 |
| 7N | 0.002475 |
| 8N | -0.100209 |
| 9Sc | -0.037826 |
| 10Se | -0.010151 |

## References in Supplementary Information

S1 G. Kresse, J. Furthmuller, *Comp. Mater. Sci.*, 1996, **6**, 15-50.

S2 G. Kresse, J. Furthmuller, *Phys. Rev. B*, 1996, **54**, 11169-11186.

S3 J. Zhou, G. Chen, K. Wu, Y. Cheng, *J. Phys. Chem. C*, 2013, **117**, 12991-12999.

S4 D. Zhao, C. Dong, B. Wang, C. Chen, Y. Huang, Z. Diao, S. Li, L. Guo, S. Shen, *Adv.*

*Mater.*, 2019, **31**, 1903545.

S5 H. Yu, R. Shi, Y. Zhao, T. Bian, Y. Zhao, C. Zhou, G. I. N. Waterhouse, L. Wu, C. Tung, T. Zhang, *Adv. Mater.*, 2017, **29**, 1605148.

S6 G. Peng, L. Xing, J. Barrio, M. Volokh, M. Shalom, *Angew. Chem. Int. Ed.*, 2018, **57**, 1186-1192.

S7 X. Wen, Z. Duan, L. Bai, J. Guan, *J. Power Sources*, 2019, **431**, 265-273.

S8 C. Liu, M. Yu, H. Liang, Y. Zhou, R. Zhan, Y. Sun, D. Li, C. Liu, J. Niu, *Sep. Purif. Technol.*, 2022, **285**, 120404.

S9 M. Yu, C. Liu, X. Sun, J. Lu, J. Niu, *ACS Appl. Mater. Interfaces*, 2022, **14**, 5376-5383.

S10 C. Liu, S. Sun, M. Yu, Y. Zhou, X. Zhang, J. Niu, *Sep. Purif. Technol.*, 2023, **311**, 123359.

S11 S. Huang, Y. Wang, J. Wan, Z. Yan, Y. Ma, G. Zhang, S. Wang, *Appl. Catal. B-Environ.*, 2022, **319**, 121913.

S12 T. Cheng, H. Gao, X. Sun, T. Xian, S. Wang, Z. Yi, G. Liu, X. Wang, H. Yang, *Adv. Powder Technol.*, 2021, **32**, 951-962.

S13 X. Zhang, Y. Chen, Q. Shang, Y. Guo, *Sci. Total Environ.*, 2020, **716**, 137144.

S14 Q. Zhou, D. Zhao, Y. Sun, X. Sheng, J. Zhao, J. Guo, B. Zhou, *Chemosphere*, 2020, **252**, 126468.

S15 R. Weng, F. Tian, Z. Yu, J. Ma, Y. Lv, B. Xi, *Chemosphere*, 2021, **285**, 131542.